9-2000

The White Dwarf Cooling Age of the Open Cluster NGC 2420

Ted von Hippel
Embry-Riddle Aeronautical University, vonhippt@erau.edu

Gerard Gilmore
Institute of Astronomy, Cambridge, gil@ast.cam.ac.uk

THE ASTRONOMICAL JOURNAL, 120:1384–1395, 2000 September

THE WHITE DWARF COOLING AGE OF THE OPEN CLUSTER NGC 2420[1]

TED VON HIPPEL
Gemini Observatory, 670 North A'ohoku Place, Hilo, HI 96720; ted@gemini.edu

AND

GERARD GILMORE
Institute of Astronomy, Madingley Road, Cambridge CB3 0HA, UK; gil@ast.cam.ac.uk
Received 2000 April 14; accepted 2000 June 1

ABSTRACT

We have used deep *HST* WFPC2 observations of two fields in NGC 2420 to produce a cluster color-magnitude diagram down to $V \approx 27$. After imposing morphological selection criteria we find eight candidate white dwarfs in NGC 2420. Our completeness estimates indicate that we have found the terminus of the WD cooling sequence. We argue that the cluster distance modulus is likely to be close to 12.10 with $E(B-V) = 0.04$. With these parameters we find a white dwarf cooling age for NGC 2420 of 2.0 ± 0.20 ($1\ \sigma$) Gyr. The 0.20 Gyr uncertainty includes errors in the photometry, sequence fitting, precursor timescales, and theoretical white dwarf cooling timescales. Comparing the cluster white dwarf cooling age to ages derived from stellar isochrone fitting we find a preference for ages derived from models incorporating convective overshoot.

Key words: Galaxy: stellar content — open clusters and associations: individual (NGC 2420) — stars: evolution — white dwarfs

1. INTRODUCTION

NGC 2420 has been the subject of numerous investigations primarily due to its combination of richness and age. Richness, of course, allows one to find stars in many of the rarer stages of stellar evolution, and in turn make detailed comparisons between stellar evolution models and the properties of either individual stars or the cluster as a whole via the cluster color-magnitude diagram (CMD) and luminosity function (LF). NGC 2420 is roughly 2 Gyr old, placing it on a logarithm age scale approximately evenly between the ubiquitous young open clusters such as the Hyades and the oldest star clusters known, the Galactic globular clusters. Overall, stellar evolutionary theory is in an advanced state with sophisticated predictive abilities, including ages that are rapidly becoming more reliable (e.g., Pols et al. 1998; Dominguez et al. 1999). A number of important uncertainties remain in stellar evolution theory, however. One of the two biggest uncertainties is the calibration between the theoretical temperature-luminosity plane and the observational color-magnitude plane. The other of the two biggest uncertainties is the theory of convection (note, however, the recent advances of Canuto and coworkers; e.g., Canuto 1999; Canuto & Dubovikov 1998), relevant both near the surfaces of stars with $T_{\rm eff} \leq 6500$ and in the cores of stars more massive than the Sun. Because of its age—and therefore the mass of stars currently evolving off the main sequence—NGC 2420 provides an important test of the degree of convection in stellar cores. The details of convection in stellar cores, in turn, have important ramifications throughout astronomy.

Recent work in cosmology and galaxy evolution has led to increased interest in stellar evolutionary ages. For galaxy evolution studies much current effort is being placed on determining the initial epoch of galaxy building and star formation. All of these studies rely on evolutionary timescales set by stellar evolution.

Because of the importance of stellar ages we have sought to test stellar evolution theory itself from outside the traditional approaches. Traditional tests of stellar evolution are based on using stellar evolution models to reproduce the properties of stars in stellar clusters and binary pairs. White dwarfs (WDs), on the other hand, can be used as chronometers with almost complete independence from the theory of main-sequence stellar evolution. There is a well-defined relation between the luminosity and age of a white dwarf (e.g., Iben & Tutukov 1984; Wood 1992; Salaris et al. 1997), especially during the first few billion years of WD cooling before crystallization effects become important. White dwarfs have been recognized as potential Galactic chronometers since at least the proposal by Schmidt (1959) that the age of the Galactic disk could be found via the luminosity limit of local WDs. Subsequently a number of studies (e.g., Winget et al. 1987; Liebert, Dahn, & Monet 1988; Wood 1992; Oswalt et al. 1996; Leggett, Ruiz, & Bergeron 1998) of the WD LF have measured the age of the Galactic disk. White dwarfs have also been found in clusters ranging in age from the Pleiades (one WD in this $\approx$70 Myr old cluster) to the globular clusters. White dwarf cooling ages have been derived for numerous young clusters, e.g., NGC 2451 (Koester & Reimers 1985), as well as a few clusters of intermediate age, e.g., Praesepe (Claver 1995), NGC 2477 (von Hippel, Gilmore, & Jones 1995, hereafter Paper I), NGC 2420 (Paper I), and M67 (Richer et al. 1998). In addition, lower limits that do not yet test stellar evolution theory have been derived via WD cooling ages for NGC 188 (von Hippel & Sarajedini 1998) and M4 (Richer et al. 1997). A number of other open and globular clusters are also known to contain WDs. For a recent summary of known cluster WDs, see the compilation of von Hippel (1998).

[1] Based on observations with the NASA/ESA *Hubble Space Telescope*, obtained at the Space Telescope Science Institute, which is operated by the Association of Universities for Research in Astronomy, Inc., under NASA contract NAS 5-26555.

Overall, there is a clear consistency between the WD cooling ages and the isochrone ages, which is comforting to note. Within this overall consistency, however, there are stellar evolution models with ages that either do or do not closely match the WD cooling ages. In this paper we make a detailed comparison between the WD cooling age we derive for NGC 2420 and nine modern isochrone ages. From this comparison we find that models with convective core overshoot are favored over canonical (no convective core overshoot) models for this cluster.

In order to avoid confusion, we note that some authors (e.g., Trimble & Leonard 1996; Dominguez et al. 1999) interpreted the WD ages we (von Hippel et al. 1995) derived for NGC 2420 and NGC 2477 as inconsistent with any isochrone ages for these clusters. Certainly, there was no consistency between the isochrone ages available at that time and our WD age for NGC 2477. On the other hand, in 1995 there were no modern isochrone studies for NGC 2477. At that time, the most recently derived age for NGC 2477 (Carraro & Chiosi 1994) was not based on isochrone fitting, but rather on an isochrone-based calibration of the magnitude difference between the main-sequence turn off and red clump luminosity. An improved WD age with a more detailed analysis of NGC 2477 will be the subject of a future study. For the present study we focus on NGC 2420, where the isochrone and WD age comparisons yielded ambiguous results in Paper I. The primary purpose of Paper I was to show the power of using WD cooling timescales as an independent test of ages derived from stellar evolutionary theory. We will show here that the increased reliability of the observational results for NGC 2420, as well as the large body of new theoretical work for this cluster, makes it worthwhile to recompare the WD and isochrone ages for this cluster. Finally, we note that the current paper supersedes Paper I as it contains more and deeper observations obtained with an improved observational technique, and it is based on a much-improved understanding of the WFPC2 calibration. Paper I was based on data taken within three months of the installation of WFPC2, before calibrations were well established.

2. OBSERVATIONS AND REDUCTIONS

We observed a single field in NGC 2420 with the *Hubble Space Telescope* (*HST*) and the then new Wide Field Planetary Camera 2 (WFPC2) in cycle 4. These observations were designed to find white dwarfs in NGC 2420 to the terminus of the cooling sequence. Limited experience with WFPC2 at that time resulted in a data set in which hot and warm pixels were hard to distinguish from faint white dwarf candidates. Our study of the cluster WDs and their implied age was presented in Paper I. After our experience with the cycle 4 data it became clear that a reliable determination of the terminus of the WD cooling sequence required dithered observations as well as twice the number of cluster stars.

In cycle 6 we obtained two additional V-band (F555W) pointings on our cycle 4 field (hereafter field 1), each slightly offset from the other and from the cycle 4 pointing. We also obtained new V- and I-band (F814W) observations of a second field (hereafter field 2). We obtained a slightly different set of individual exposure lengths and total exposure times for field 2, based on our experience with field 1. The details of the observations are given in Table 1. The first column of Table 1 lists the dates of the nine different NGC 2420 pointings. The second column lists the number of exposures and the length of each exposure in seconds. The last five entries indicate three exposures composed of individual exposures of both 700 and 800 s. The third column lists the WFPC2 filter used, the fourth column lists the observed sky value in counts, the fifth column lists the field identifier we use throughout the text, and the sixth column lists the *HST* cycle number in which the observations were made. Fields 1 and 2 are centered 3.′4 southwest and 1.′4 northeast of the apparent cluster center at $7^h38^m11^s.2$, $+21°33'09''.7$ and $7^h38^m28^s.5$, $+21°35'29''.1$ (J2000.0), respectively.

TABLE 1

LOG OF OBSERVATIONS

Date (1)	Exposures (s) (2)	Filter (3)	Sky (4)	Field (5)	Cycle (6)
1994 May 18...	4 × 900	F555W	33.6	1	4
1994 May 19...	4 × 900	F814W	33.2	1	4
1996 Apr 2.....	2 × 1200	F555W	16.8	1	6
1996 Apr 2.....	2 × 1200	F555W	17.0	1	6
1997 Apr 3.....	3 × 700/800	F555W	11.7	2	6
1997 Apr 3.....	3 × 700/800	F555W	11.7	2	6
1997 Apr 3.....	3 × 700/800	F555W	11.6	2	6
1997 Apr 3.....	3 × 700/800	F814W	11.1	2	6
1997 Apr 3.....	3 × 700/800	F814W	11.1	2	6

We recalibrated the entire data set using the Canadian Astronomy Data Centre's[2] archive pipeline with up-to-date calibration files. Following recalibration, we stacked the aligned images of each subfield and rejected the cosmic rays with the IRAF[3] task CRREJ. Since there were only a few stars in the PC frames we dropped the PC frames of both fields from all further reduction and analysis. We then used the drizzle package (Fruchter & Hook 1998) to shift and stack the dithered WF frames to arrive at a combined V and a combined I frame for each of fields 1 and 2. The drizzle process rejected most hot pixels and other image defects and produced reasonable stellar point-spread functions (PSFs). The PSFs were sometimes a bit distorted, due probably to the fact that there were only two or three pointings per filter per field. The effect of the PSF shapes on the quality of the photometry was small, as will be discussed below. The primary purpose for obtaining dithered observations and incorporating drizzled reductions was to remove the hot pixels, which worked well. We employed SExtractor (Bertin & Arnouts 1996) to find and classify sources and CCDCAP[4] (Mighell 1997), an aperture photometry task specifically designed for WFPC2 data, to derive instrumental magnitudes.

As is well known by now, a number of small corrections must be applied to WFPC2 photometry to fully remove instrumental artifacts. We endeavored to apply these corrections as best we could based on the current knowledge of the WFPC2 instrument. The effect of geometrical distortions on the WFPC2 photometry was corrected by drizzle.

[2] CADC is operated by the Herzberg Institute of Astrophysics, National Research Council of Canada.

[3] IRAF is distributed by the National Optical Astronomy Observatories, which are operated by the Association of Universities for Research in Astronomy, Inc., under cooperative agreement with the National Science Foundation.

[4] IRAF implementations of CCDCAP are available at http://www.noao.edu/staff/mighell/ccdcap/.

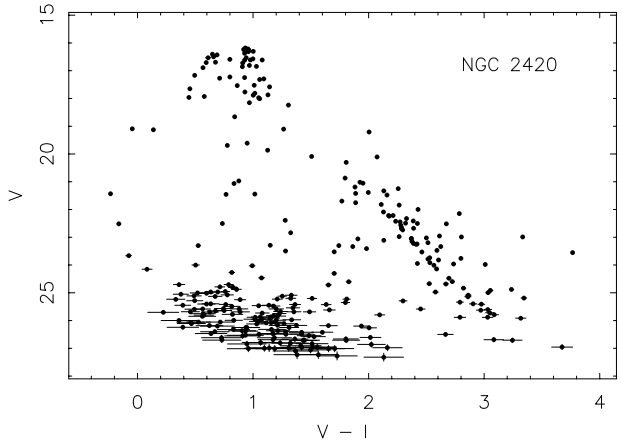

FIG. 1.—NGC 2420 CMD. All objects with σ_V and $\sigma_I \leq 0.15$ mag are plotted, along with their 1 σ error bars. No cut is made on image morphology.

To remove the effects of the charge transfer (in)efficiency (CTE) problem we used the algorithms of Stetson (1998) and Whitmore, Heyer, & Casertano (1999). The Whitmore et al. CTE algorithm is independent of the so-called "long versus short exposure effect," which we corrected using the prescription of Casertano & Mutchler (1998). Both the Stetson (1998) and Whitmore et al. (1999) plus Casertano & Mutchler (1998) approaches gave typical corrections rising from ≈ 0.02 mag at V or $I = 16$ to ≤ 0.10 mag at V or $I = 26$. While these two approaches differ in mathematical form and only the latter corrects the time-dependent nature of the CTE, for our data they both gave very similar results. The mean V magnitude difference between these two approaches among the faint ($V = 22$ to 26) stars is ≤ 0.01 mag. We take this small difference as an indication that we have reliably corrected the effects of CTE, with an estimated uncertainty in this correction no more than double the difference between these two prescriptions, i.e., ≤ 0.02 mag.

To determine the photometric drift of the WFPC2 with time we analyzed the relevant calibration data.[5] For the epochs of our observations the corrections were always $\leq 1\%$, except for WF3 at one epoch (1996 April 2), which required corrections of $+1.5\%$ and $+2.0\%$ in F555W and F814W, respectively. We chose only to correct these two cases where the photometric drifts had exceeded 1%. Since even these frames were combined with other frames from epochs with essentially no photometric drift, the resulting corrections were only 0.005 and 0.0067 mag in F555W and F814W, respectively. The error on these corrections is likely to be ≤ 0.002 mag.

The fairly large number of well-exposed stars on each WF chip allowed us to measure aperture corrections for each combination of WF chip, filter, and field. The aperture corrections had typical errors of 0.01 to 0.015 mag. We also investigated whether there were any spatially dependent aperture corrections and found none. We did not apply any breathing corrections to the photometry. The fact that neither spatially dependent aperture corrections nor breathing corrections were necessary was most likely due to the fact that each combined image represented from four to 10 exposures covering always more than one orbit. We also did not apply corrections for the photometric offsets due to pixel size differences at every 34th row (Anderson & King 1999). Although this correction statistically affects 6% of the stars by 0.01 to 0.02 mag, the manner in which we combined our photometry with drizzle meant that the 34th row effect would induce errors in 18% of our photometry, but only by 0.003 to 0.007 mag.

Finally, the data were transformed to the Johnson V and Kron-Cousins I system via the equations of Holtzman et al. (1995). While the F555W and F814W filters transform well to the standard V- and I-band system, there is naturally an error associated with this step as well, estimated to be $\approx 2\%$ (Holtzman et al. 1995). The Holtzman et al. photometric transformations are applicable over the color range $-0.3 < V-I < 1.5$, whereas our stars continue to $V-I \approx 3.2$. The emphasis in this paper is on the cluster white dwarfs, which are within the color limits of the Holtzman et al. transformations.

Our photometry is presented in Figure 1, where the error bars represent only the internal, statistical photon-counting error. The external systematic error in the important cool WD region of the color-magnitude diagram, near $V = 25.6$ and $V-I = 0.6$, is the quadrature sum of the above errors, and amounts to ≈ 0.03 mag. The dominant sources of systematic error are the CTE corrections and the photometric transformations.

3. DISCUSSION

3.1. *The Color-Magnitude Diagram*

There are a large number of galaxies and remaining image defects with the approximate color and magnitude of the faint WDs in NGC 2420 (Fig. 1). One of the major motivations for using *HST* for this study is the ability of this telescope to resolve nearly every galaxy in the universe, when sufficient signal-to-noise is obtained. Thus, if image defects can be eliminated any unresolved object is almost surely a star. The converse of this is also true, any resolved object, even marginally resolved, is not a star. For our purposes, we required good galaxy and image-defect rejection beyond the limit of the WD cooling terminus, at $V \approx 25.6$. Our data are of sufficient quality to do this, and the SExtractor classifications provided an easy means of making this separation.

Figure 2 shows the results of the SExtractor morphological classification versus V-band magnitude. The "stellarity index" ranges from 0 (galaxies) to 1 (stars). Careful examination of the images revealed that all objects with stellarity index ≥ 0.9 are unresolved (i.e., stars). Objects with stellarity indices between 0.9 and 0.6 are a mixture of unresolved objects, very faint objects, and image defects. All objects with stellarity index ≤ 0.2 are resolved, although some are not galaxies, but rather ghost images or diffraction spikes. Objects with stellarity indices between 0.5 and 0.2 are a mixture of resolved objects, very faint objects, and image defects. The term "image defects" here is meant to include the remaining hot and warm pixels, as well as residual remaining cosmic rays, ghost images, diffraction spikes, etc.

The large number of definite stars near the top of Figure 2 demonstrates that a star cluster is present in this field. Contamination by background galaxies becomes significant at $V \approx 25$, and near $V = 27$ a combination of objects too faint to reliably classify and image defects predominate.

[5] See Standard Star Monitoring Memo at http://www.stsci.edu/instruments/wfpc2/Wfpc2_memos/wfpc2_stdstar_phot3.html.

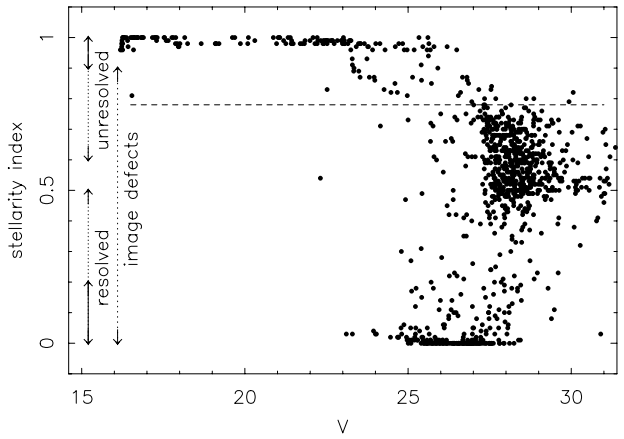

FIG. 2.—Apparent V magnitude vs. the SExtractor (Bertin & Arnouts 1996) stellarity index. The stellarity index ranges from 1.0 for definite unresolved objects to 0.0 for definite resolved objects. The horizontal dashed line at 0.78 is our stellar classification threshold. The vertical arrows on the left indicate ranges for resolved and unresolved objects, as well as image defects and noise. *All* objects with a stellarity index ≥ 0.9 are clearly unresolved and *all* objects with a stellarity index ≤ 0.2 are clearly resolved. These areas of certainty are indicated by the solid vertical arrows. The dashed vertical arrows indicate areas of parameter space where *some* objects are either clearly resolved or clearly unresolved.

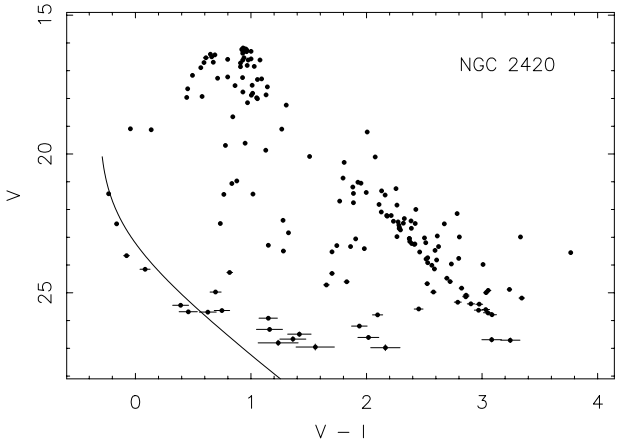

FIG. 3.—NGC 2420 CMD after removal of all resolved objects and image defects. Only objects with σ_V and $\sigma_I \leq 0.15$ mag and with a stellarity index ≥ 0.78 are plotted. The line is a cooling track for a 0.7 solar mass C-O WD (Benvenuto & Althaus 1999) placed at a cluster distance modulus of 12.10.

Note also that saturated stars have a stellarity index of somewhat less than 1.0 due to their flat-topped, broader PSFs. The stellarity index cut of 0.78 is drawn in Figure 2. This choice was somewhat relaxed from the classification value for a typical well-exposed star since the drizzle processing created some slightly distorted PSFs. To be considered a star, an object had to have a stellarity index of ≥ 0.78 in either the V- or the I-band frames. By allowing the classification to be based on either frame, we were able to bypass some of the reduced classification probabilities due to the distorted PSFs caused by the drizzle process, as well as take into account that some of the faintest stars are better observed in one filter than the other, depending on their color. Nonetheless, we tried to be conservative for each of the stars that matter in this study, i.e., the WDs, and we additionally examined each of these detections by eye to check for adjacent image defects, crowding with stars or galaxies, or any other problem that might compromise the morphological classifications or the photometry. The subject of morphological classification and how one compromises between ensuring that only stars are counted and ensuring that no stars are missed will be revisited in § 3.3. For now we take all objects with a stellarity index ≥ 0.78 as stars and plot them in Figure 3.

The reader might wonder whether proper motions could be used in this cluster to help differentiate members from nonmembers. While it is true that our field 1 observations span a period of two years, all of our field 2 observations were obtained on the same day (see Table 1). Furthermore, the proper motion of the cluster is known to differ from the mean proper motion of bright ($B \leq 13.5$) stars in this field by $\approx 0\farcs002$ yr^{-1} (van Altena & Jones 1970), or only 0.04 WF pixels over a 2 yr baseline. The primary difference between the cluster and field is in the dispersion of proper motions, with measured values corresponding to 0.014 and 0.064 WF pixels over the two-year baseline for the cluster and field stars, respectively. We were thus not surprised when we were unable to detect a difference between cluster and field stars in field 1 based on the change in image centroids. Our typical measuring error appeared to be ≈ 0.1 pixel. These errors could perhaps be reduced by deriving optimized centroids, but we judged the likely additional information to be minimal. Fortunately, proper motion information is not required as there are few remaining contaminating objects, either Galactic field stars or unresolved background galaxies, in the WD portion of the CMD (Fig. 3).

The CMD presented in Figure 3 shows a clear main sequence extending 10 mag from $V \approx 16$ to $V \approx 26$. The apparent gap in the main sequence from $V \approx 19$ to 21 is likely just a statistical variation in the cluster luminosity function for our two fields, visually exaggerated by the pile up of saturated photometry near $V = 16$. Wider field coverage of NGC 2420 would demonstrate whether this gap is a real and unexpected variation in the cluster LF. Note that the ground-based CCD photometry of Anthony-Twarog et al. (1990), which covered 20 times as much of the cluster as our study, does not show this gap, though part of the gap is beyond the limit of their photometry. Regardless of the astrophysical meaning of the gap, it is not caused by any form of incompleteness in the *HST* photometry. Even stars one magnitude fainter than the bottom of the gap are readily visible to the naked eye in the raw uncombined images even before cosmic ray rejection.

The two separate clumps of saturated stars are the result of our use of exposure times ranging from 700 to 1200 s in F555W. The cluster main-sequence binaries are also visible, particularly between $V = 21$ and 24. In the lower left of the CMD a series of blue stars from $V \approx 21.4$ to 25.6 closely follow the cooling track for a 0.7 solar mass carbon-oxygen WD model (Benvenuto & Althaus 1999). The WD model was placed at a distance modulus of 12.10 (see § 3.2). There are also a few dozen stars sprinkled throughout the CMD between the WD sequence and main sequence. These are Galactic field stars behind the cluster.

As a final tool to understanding objects in the observed CMD (Fig. 3) we employed the Galaxy model of Reid & Majewski (1993) to create a model CMD for Galactic field stars at the location of NGC 2420. This model has been tested against north Galactic pole number counts and color

distributions (Reid & Majewski 1993) and against two deep, lower latitude fields (Reid et al. 1996). The model CMD is presented in Figure 4. Note that the model predicts that there should be some Galactic field stars near the cluster main sequence and a few more sprinkled in the region between the main sequence and the WD sequence, roughly as seen in the observed CMD. By increasing the model normalization by a factor of 10 we find the model predicts that 0.6 Galactic disk WDs lie somewhere along the observed cluster WD sequence. This implies that there may be a single interloper somewhere along the cluster WD cooling sequence. The likelihood of a Galactic WD interloper in the magnitude beyond the observed WD cooling sequence limit is much lower, however, as only 0.2 WD interlopers are expected in this region. We do not want to over-interpret this model-dependent estimation of the numbers of WD interlopers, however, i.e., by claiming that a $+4$ σ enhancement in Galactic WD numbers would be required in this field to contaminate the WD terminus, since the Reid & Majewski model has never been tested on faint field WDs. We are simply using these model predictions to argue that it is unlikely that a Galactic field WD is among the faintest observed WDs in our CMD. We further note that such an interloper need not affect the derived cluster WD cooling age if the cluster age is determined from WD isochrone fitting, rather than from just the faintest WD (see § 3.3).

3.2. *Cluster Parameters*

The most commonly used values for the distance modulus and reddening for NGC 2420 are $(m - M)_V = 11.95$ and $E(B-V) = 0.05$, values largely supported by the data and analysis of Anthony-Twarog et al. (1990). Anthony-Twarog et al. fit VandenBerg (1985) isochrones to their photometry. Are results derived from these older models still the most reliable? Indeed, Anthony-Twarog et al. noted the poor fit between the cluster turn-off region and the VandenBerg (1985) isochrones. Subsequent reanalysis of the Anthony-Twarog et al. data by Demarque, Sarajedini, & Guo (1994), incorporating up-to-date stellar evolution models, yielded $(m - M)_V = 12.05 \pm 0.10$ and $E(B-V) = 0.045^{+0.020}_{-0.015}$. In another reanalysis, Twarog, Anthony-Twarog, & Bricker (1999), in a detailed study of the red giant clump luminosity in NGC 2420 and other open clusters, employed stellar evolution models and main-sequence fitting to rederive the parameters for NGC 2420. Twarog et al. argued that $(m - M)_V = 12.15$ and $E(B-V) = 0.04$. We take these two analyses as being the most up-to-date and conclusive on the issue of the cluster distance and reddening, and adopt the mean of their distance moduli, 12.10. The reddening values for the two studies are entirely consistent, and we adopt $E(B-V) = 0.04$.[6] In the analysis of the WD cooling ages, below, we will determine WD age as a function of assumed distance modulus since a wide range of distance moduli have been used in the isochrone fits. The value of the reddening does not affect the cluster WD ages since the WD isochrone fits depend almost entirely on V luminosity, and not color. It is comforting to note, however, that the cluster reddening is low and consistent in these modern studies.

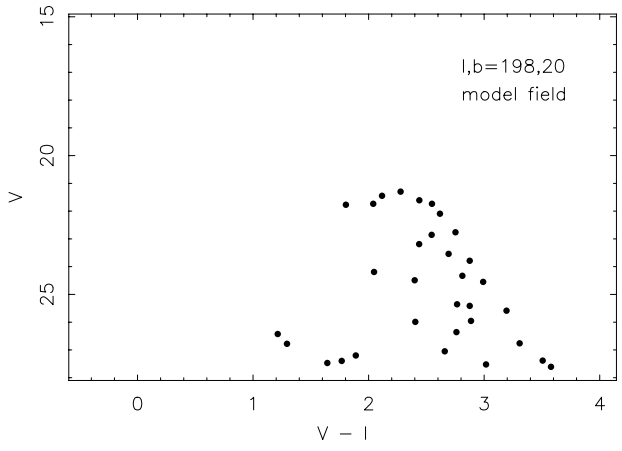

FIG. 4.—CMD for the Galaxy model of Reid & Majewski (1993) for the location ($l = 198$, $b = 20$), sky coverage, and reddening of our NGC 2420 fields.

We derived an independent distance modulus by fitting the open cluster fiducial main sequence presented by Pinsonneault et al. (1998) to the Anthony-Twarog et al. data. We found a distance modulus of 11.85 to 12.02 for [Fe/H] $= -0.4$ and 11.95 to 12.10 for [Fe/H] $= -0.3$. Our distance modulus is consistent with that of Twarog et al. (1999) given their assumed metallicity, [Fe/H] $= -0.29$. Rather than using the distance modulus we obtained from main-sequence fitting, we rely on the above average distance modulus of 12.10, since the main-sequence fitting technique is so sensitive to the cluster metallicity.

3.3. *White Dwarfs*

In Paper I (see Fig. 2 of that study) we found five WD candidates in the single *HST* pointing. We recovered all five of these WD candidates in our present analysis but only three of them (and only one of the faintest three from Paper I) passed our morphological classification. We imposed tighter constraints in this study since we have both more data and a greater knowledge of our data. The two objects excluded may very well be cluster WDs and may just have slightly deviant PSFs due to the drizzle processing. Regardless of the cause, we wanted to minimize suspect objects, and so do not include these objects in the CMDs of Figures 2 and 3. We note, however, that the V-band luminosities for these two rejected potential WDs ($V = 25.28$ and 25.16 in our present data, $V = 25.11$ and 24.87 in our cycle 4 reductions) are 0.4 mag brighter than the faintest WDs presented here. Their inclusion would not affect our derived WD age. Our candidate WDs are listed in Table 2. Column (1) lists a WD identification number, ordered by brightness in the V-band. Column (2) lists the object V magnitude, followed by its uncertainty in column (3). Column (4) lists the $V-I$ color, followed by its uncertainty in column (5). Columns (6) and (7) list the object's right ascension and declination (J2000.0), respectively. The errors in position are expected to be $\approx 0\farcs5$. The relative positions of objects in the same WFPC2 field should be significantly more accurate, $\approx 0\farcs1$.

Of the eight candidate WDs presented in Table 2 and Figures 2 and 3, one candidate (WD4) had a significantly lower probability (0.71 in V, 0.23 in I compared with our threshold value of 0.78) of being stellar, according to the SExtractor stellarity index. We nonetheless retain this object since we believe its morphological classification

[6] In Paper I we adopted $(m - M)_V = 11.95$ and $E(B-V) = 0.05$.

TABLE 2

WHITE DWARFS

ID (1)	V (2)	σ_V (3)	$V-I$ (4)	σ_{V-I} (5)	R.A. (6)	Decl. (7)
WD1.....	21.43	0.003	−0.23	0.009	7 38 10.62	21 32 33.5
WD2.....	22.52	0.005	−0.16	0.016	7 38 08.07	21 33 08.8
WD3.....	23.66	0.010	−0.08	0.025	7 38 26.54	21 35 13.1
WD4.....	24.15	0.015	0.08	0.044	7 38 10.85	21 31 56.6
WD5.....	25.45	0.032	0.39	0.069	7 38 31.26	21 35 56.6
WD6.....	25.64	0.038	0.75	0.067	7 38 29.68	21 36 45.4
WD7.....	25.68	0.038	0.46	0.079	7 38 30.50	21 34 31.3
WD8.....	25.69	0.039	0.63	0.073	7 38 30.12	21 36 34.0

NOTE.—Units of right ascension are hours, minutes, and seconds, and units of declination are degrees, arcminutes, and arcseconds.

appears nonstellar due to crowding by an adjacent galaxy. Furthermore, upon carefully examining this object in the V- and I-band images, it appeared that the crowding galaxy had a similar color and is unlikely to greatly change the derived color of this candidate WD. Since we believe it is a WD and since the hotter WDs hold none of the weight in the age fit, we present it in our CMDs.

Before applying WD isochrones to our data, we first discuss the inputs required for the WD isochrones. First, we require a cluster distance modulus to convert apparent magnitudes to absolute magnitudes. Second, we require the evolutionary ages of the precursor stars, including the time required for them to evolve from the main sequence through the giant branch, through any subsequent burning stages, and through the planetary nebula stage until they become WDs. For precursor ages we rely on the stellar evolution parameterizations of Hurley, Pols, & Tout (2000). To connect the precursor masses to the WD masses, we employ the initial–final mass relation of Wood (1992). Other modern studies (e.g., Koester & Reimers 1996; Dominguez et al. 1999) of the initial–final mass relation are consistent at the level required for our purposes.

It may seem counterintuitive that ages derived via WD luminosities could be independent of stellar evolution theory since the total age of the WD depends on the precursor ages, but the rapid evolution of high-mass stars means that the precursor timescales have little leverage on the total age. The WDs that are presently the coolest and faintest in any cluster are those which formed first and therefore those which evolved from the most massive progenitors. The first stars to become WDs had a main-sequence mass somewhere between 6 and 8 solar masses with total evolutionary timescales of $\leq 8 \times 10^7$ yr, i.e., $\leq 5\%$ of the ≈ 2 Gyr ages considered here. In order to quantify the uncertainty in the WD ages due to the uncertainty in the precursor lifetimes, we measured the difference in total age after adjusted the precursor masses by $\pm 20\%$. This change in precursor mass should account for both uncertainty in the initial–final mass relation and uncertainty in the evolutionary timescales themselves. For example, the Wood initial–final mass relation gives a precursor of 3.67 solar masses for a 0.7 solar mass WD. The $\pm 20\%$ mass values become 4.40 and 3.06 solar masses and the evolutionary timescales of these stars are 0.160 and 0.412 Gyr (Hurley et al. 2000). For a 0.9 solar mass WD the $\pm 20\%$ precursor mass values correspond to evolutionary timescales of 0.048 to 0.104 Gyr. These evolutionary timescales vary by a factor of more than 2, yet the effect of these precursor timescale changes, weighted among WDs of different masses, results in a cluster WD age uncertainty of only -0.05, $+0.07$ Gyr. Clearly, for clusters of ≈ 2 Gyr, realistic uncertainties in precursor timescales are unimportant, and thus the cluster WD age is essentially independent of stellar evolution theory.

As a check on the reliability of the WD cooling theory itself, we compared the WD cooling models of different groups. Since the Wood (1992) models were provided to us in the form of WD isochrones (Ahrens 1999) we use them as our fiducial set. The Benvenuto & Althaus (1999) and Hansen (1999) models are in the form of cooling tracks for WDs of different masses. To these cooling models we added the precursor timescales from Hurley et al. (2000), as discussed above. Within the age range of 1.5 to 2.5 Gyr, as given by the Ahrens isochrones, we found that the Benvenuto & Althaus models were systematically older than the Ahrens isochrones by 0.18 Gyr, and the Hansen models were systematically older than the Ahrens isochrones by 0.05 Gyr. Rather than use an average result from the three different sets of models, we use the Ahrens isochrones to derive our cluster WD age and use the differences between the models as an indication of the uncertainties in the WD cooling timescales. We estimate the age uncertainty to be ≈ 0.15 Gyr within the theoretical models themselves, for clusters between 1.5 and 2.5 Gyr.

Although we believe the morphology cut we have chosen properly separates stars from galaxies, we now demonstrate the insensitivity of our results to the chosen morphological cut. The general issue is somewhat complicated and depends on the goal of the particular study. If we wished to derive a minimum cluster age then we would need to reject every possible galaxy and use only objects that are highly likely to be white dwarfs. On the other hand, if we wished to derive a maximum cluster age then we would need to include any object that might be a cluster white dwarf. Even without the image morphology information, the shape of the WD LF provides additional guidance, and as our analysis will show, the minimum and maximum WD age are one and the same for these data.

Figure 5 presents all possible candidate WDs in our two fields. These objects are selected based on their photometric proximity (1.5 σ) to the model cooling tracks for 0.6 to 1.0 solar mass carbon-oxygen WDs (Benvenuto & Althaus 1999) placed at the cluster distance. The symbols indicating the range of the stellarity index value, with the filled symbols indicating the most reliable WD candidates. Recall that objects with stellarity index ≤ 0.2 are obviously resolved to the eye, and so we do not include them in Figure 5. In

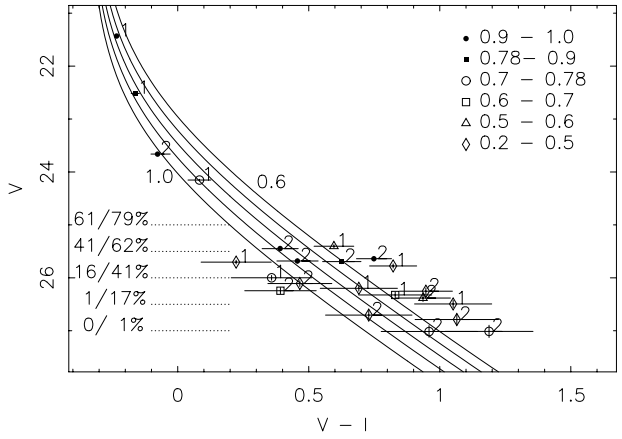

FIG. 5.—WD portion of the CMD displaying all possible WD candidates. Objects were selected based on their photometric proximity (1.5 σ) to the model cooling tracks for 0.6 to 1.0 solar mass C-O WDs (Benvenuto & Althaus 1999) placed at the cluster distance. The symbols indicate the stellarity index range. Objects with stellarity index ≤ 0.2 are obviously resolved to the eye and therefore are not plotted. The dotted lines in the lower left are the probabilities of finding objects as a function of luminosity, with the first and second numbers indicating completeness in fields 1 and 2, respectively. Each object is labeled with the field in which it was found.

fact, objects within the $0.2 \leq$ stellarity index ≤ 0.5 range are almost surely all galaxies or image defects, but we include them in our analysis anyway, in order to demonstrate that this form of noise will not approximate the shape of a WD LF. The dotted lines in the lower left of Figure 5 are the probabilities of finding objects as a function of luminosity, with the first and second numbers indicating completeness in fields 1 and 2, respectively. Since the completeness levels are different in fields 1 and 2, each object is labeled with the field in which it was found.

The completeness estimates presented in Figure 5 were determined by scaling artificial star tests we performed on our cycle 4 data in Paper I using the TinyTim package (Krist 1995). Reproducing artificial star tests for our combined, dithered and drizzled, cycles 4 plus 6 observations would have been laborious, but fortunately was unnecessary. The cycles 4 and 6 observations were obtained with the WFPC2 in exactly the same configuration. Additionally, the faintest stars, i.e., those for which the issue of completeness is the most relevant, are faint enough that sky noise dominates shot noise in the object by a factor of 2 and read noise by a factor of 4 to 6. We were thus able to scale our earlier completeness simulations to our combined cycle 4 plus 6 data set based on the new cumulative exposure times and sky values. We note that the limiting depth of our CMDs is not dictated by the ability of the software to find objects at a limiting flux level, but rather by the need for sufficient signal-to-noise to obtain reliable morphological classification and a photometric precision of ≤ 0.15 mag in both V and I. As it turns out, both the needed photometric and morphological precision lead to essentially the same limiting magnitude. These photometric and morphological precision cuts are the reason so few objects are seen in Figure 3 fainter than $V = 26$, even though Figure 2 shows many objects detected at fainter magnitudes.

Figures 6*a* through 6*f* presents the LFs extracted by lowering the threshold through each stellarity index cut-off for objects in field 2, with the cut-off values indicated in each panel. The bin widths are 0.25 mag to preserve the quality of the photometry and the apparent pile-up of objects near $V = 26.6$. Only objects in field 2 are presented in Figures 6*a*–6*f* as the field 2 observations probe ≈ 0.5 mag fainter than those of field 1. The cross-hatched histogram presents the observed luminosity functions, whereas the unfilled histogram presents the luminosity functions corrected for completeness. The final, corrected LF bin of each of panels (*c*) through (*f*) contains 200 objects. These panels are not rescaled to view this final bin as the rest of the LFs would be invisible. Overplotted on each panel is the WD LF derived by Richer et al. (1998) for the ≈ 4 Gyr open cluster M67. The Richer et al. WD LF is the best open cluster, i.e., single-age burst, WD LF currently available. They presented their WD LF with bin widths of 0.5 mag. Their error bars are due to both counting statistics and background subtraction errors. We normalized and slid in V magnitude the Richer et al. WD LF to match the identified LF peak. While all the panels of Figure 6 suffer from low number statistics, only Figures 6*a* and 6*b* display reasonable LFs. If one were to insist that Figures 6*e* or 6*f* contained reasonable WD LFs, two new problems would emerge. First, there should be at least half a dozen observed candidate WDs in the quarter magnitude bin just beyond the identified WD LF terminus. Perhaps this is simply due to low number statistics? Second, the LFs of Figure 6*e* and 6*f* would imply twice as many cluster WDs as main-sequence stars, which would be more than an order of magnitude more WDs than seen in any other star cluster or in the solar neighborhood (von Hippel 1998).

In summary, though we find only four objects that we identify with the WD cooling sequence terminus, we believe our identification is sound, because (1) we believe our morphological selection criteria are reasonable, (2) relaxing those morphological criteria from 0.78 to 0.7 or 0.6 does not change the WD LF, and (3) even relaxing the morphological criteria to extreme levels only creates LFs too absurd to be true cluster WD LFs.

A separate question is whether the cluster could have dynamically ejected its faintest WDs. Significant dynamical ejection of the oldest WDs is not expected, however, since these WDs have higher masses than both the younger WDs and the bulk of the main-sequence stars. Strictly speaking, the ages derived from the WD terminus provide not a cluster age, but rather a firm lower limit to the cluster age, since both photometric incompleteness and stellar ejection could rob the cluster CMD of its oldest WDs. If stars appear to pile up at an observed WD cooling sequence terminus, however, it is likely that the cluster age is equal to, or just slightly greater than, the age implied by the faintest cluster WDs.

In Figure 7*a* we present the CMD of Figure 3 with distance and reddening removed.[7] The white dwarf region of the CMD is presented in Figure 7*b*. Plotted in Figures 7*a* and 7*b* are the Ahrens isochrones abutted to a 0.6 solar mass C-O WD cooling track (Wood 1992) for 0.5, 1.0, 1.5, 2.0, 2.5, and 3.0 Gyr. The blue hook at the bottom of each isochrone and among the coolest WD candidates is the expected result of both the fact that cooling is a function of WD mass and that more massive WDs are bluer. There

[7] $E(V-I) = 1.21E(B-V)$ for the *HST* F814W filter, based on equations (3a) and (3b) of Cardelli, Clayton, & Mathis (1989).

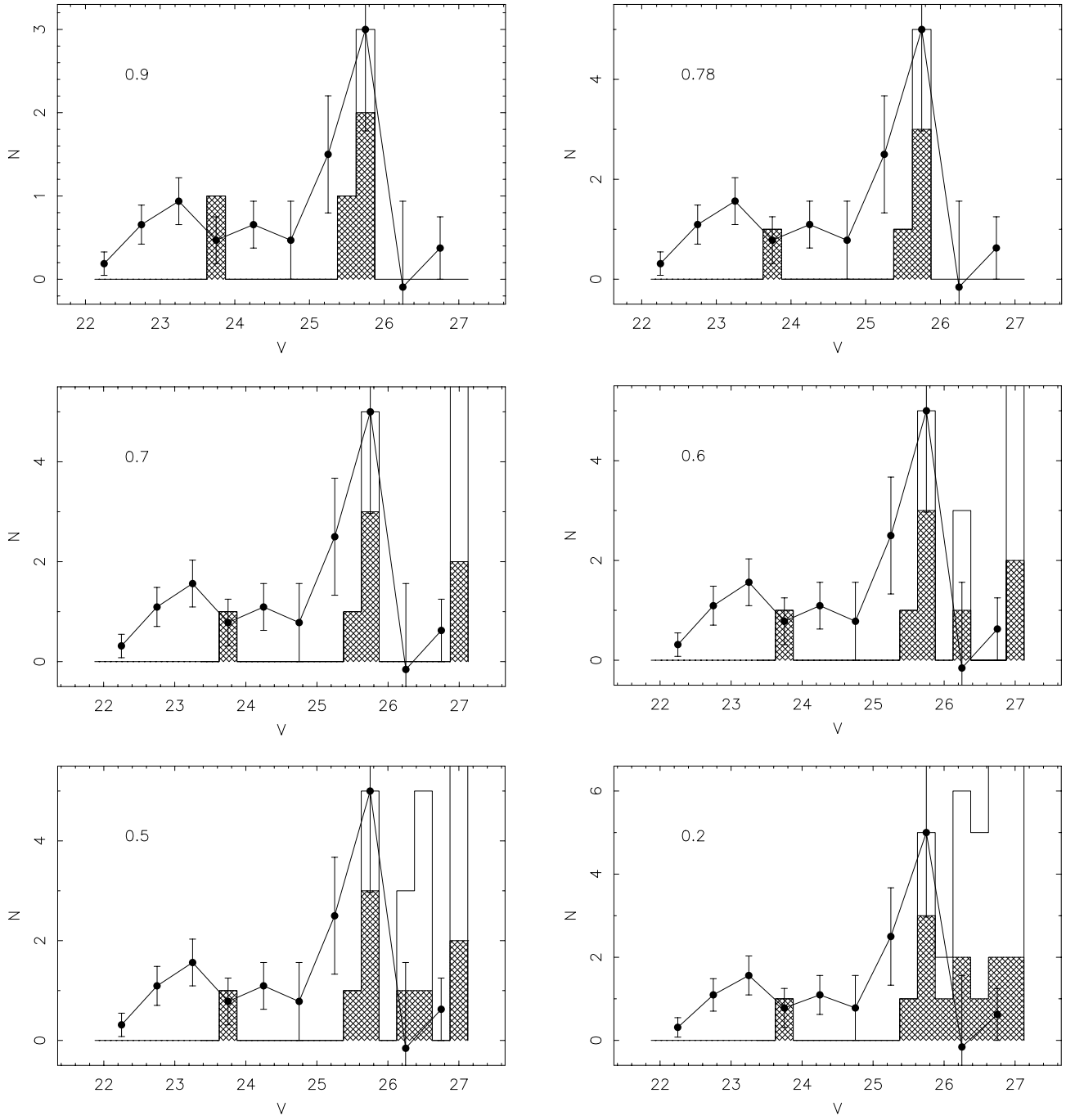

FIG. 6.—Luminosity functions of objects from Fig. 5 and field 2 above the stellarity index thresholds indicated in each panel. The cross-hatched histogram presents the observed LFs, whereas the unfilled histogram presents the completeness-corrected LFs. The final, corrected LF bin of each of panels (*c*) through (*f*) contains 200 objects. Overplotted on each panel is the WD LF of Richer et al. (1998) for the $\approx$4 Gyr open cluster M67, along with error bars due to both counting statistics and background subtraction errors.

appears to be a color offset between the reddest WD candidate and the Ahrens isochrones of $\approx$0.2 mag, though this offset depends on the assumed cluster distance. Likewise, the brightest and bluest WD is $\approx$0.03 mag redder than the Ahrens isochrones. The Ahrens isochrones differ by a few hundredths of a mag in $V-I$ color from the cooling sequences of Benvenuto & Althaus (1999) and Hansen (1999); e.g., compare the location of these objects to the WD tracks of both Figures 5 and 7*b*. The most likely explanation is that the imperfect color match between the models and candidate WDs is due to a simple combination of random and systematic photometric errors along with small uncertainties in the cooling track colors. Fortunately, the WD isochrone fit depends primarily on the theoretically and observationally more precise WD luminosities, and only secondarily on the colors.

We find a best-fit age of 2.0 ± 0.1 Gyr, not including photometric errors or errors in the distance modulus. The photometric errors for the faintest WDs range from 0.032 to 0.039, with a further systematic uncertainty in the calibration of $\approx$0.03 mag. Since all four of the faintest WDs contribute to the age derivation the total photometric

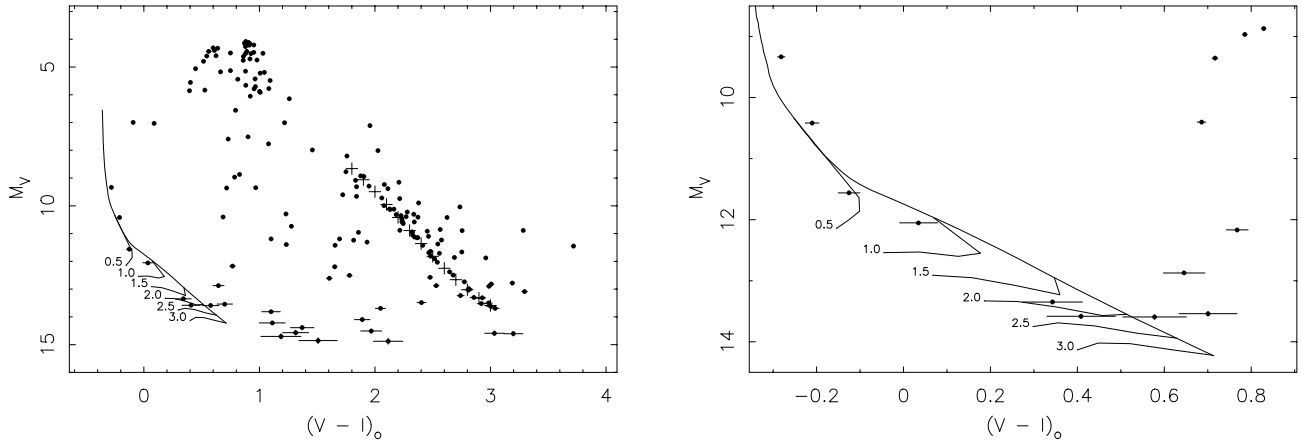

FIG. 7.—*Right*: NGC 2420 CMD with our preferred distance modulus and reddening removed. The 0.5, 1.0, 1.5, 2.0, 2.5, and 3.0 Gyr isochrones (Ahrens 1999) and 0.6 solar mass WD cooling track (Wood 1992) are over-plotted. The main-sequence ridge line is indicated by plus symbols. *Left*: Same as right panel, but only showing the WD region of the CMD.

uncertainty is ≈ 0.05 mag, corresponding to an age uncertainty of ≈ 0.06 Gyr. Combining the photometric, fitting, precursor, and theoretical errors in quadrature we arrive at a best-fit cluster age of 2.0 ± 0.20 ($1\ \sigma$) Gyr, for $(m - M)_V = 12.10$ and $E(B-V) = 0.04$. We do not consider isochrone fits for WDs with helium atmospheres since most WDs in this luminosity range have hydrogen atmospheres. We also do not consider errors in the distance modulus in deriving a best age for NGC 2420 since it would be unfair to compare a WD age derived with a certain distance modulus with the various isochrone fitting studies which have assumed different distance moduli. In our comparisons between the cluster WD and main-sequence ages in the next section we instead derive a best-fit age for a range of cluster distance moduli.

3.4. *Isochrone Ages*

Determining a best value for the cluster isochrone age is complex. Indeed, the complexity and importance of the age question is the reason why we have chosen to apply the WD cooling age technique to this cluster. Because of its age, NGC 2420 is an excellent candidate to test the reality and, if real, the amount of convective core overshoot in stars of intermediate stellar mass.

In the last decade, numerous studies have addressed the question of convective core overshoot for NGC 2420 and derived ages with or without this component in their models. Earlier studies of NGC 2420 predate the entire question of convective core overshoot. Since our goal here is to compare our WD ages with those stellar evolution ages that are in current use, and in particular to address the question of convective core overshoot, we consider the isochrone ages derived only over the last decade. Table 3 summarizes the isochrone fits to NGC 2420 that meet our criteria, in chronological order first for the studies employing canonical models, then for the studies employing convective core overshoot. Column (1) lists the derived cluster age in gigayears with any reported age uncertainty in parentheses. Column (2) lists whether the stellar evolution model incorporated core convective overshoot or not. Columns (3) and (4) list the distance modulus and reddening, respectively. We do not tabulate the uncertainties in distance moduli and reddening since many authors did not report these uncertainties. Furthermore, the relevant issue for our study is to know what distance modulus corresponds to the reported age so that we can make the proper comparison between the WD and isochrone age fits. Column (5) indicates whether the distance modulus and reddening were derived ("D") along with the cluster age or adopted ("A") from other studies. The relevance of derived versus adopted cluster parameters is that the use of a highly improbably distance modulus or

TABLE 3

AGES DERIVED FROM ISOCHRONE FITS

Age (Iso) (1)	Overshoot? (2)	$(m - M)_V$ (3)	$E(B-V)$ (4)	Derived? (5)	[Fe/H] (6)	Ref. (7)	Age (WD) (8)
3.4 (0.6).....	N	11.95	0.05	D	−0.40	AT90	2.3
1.7	N	11.95	0.02	D	0.00	C92	2.3
1.6 (0.2).....	N	12.19	0.05	D	−0.40	D99	1.9
1.5 (0.1).....	N	12.40	0.16	D	−0.40	C99	1.6
2.1	Y	11.80	0.08	D	−0.42	CC94	2.5
2.4 (0.2).....	Y	12.05	0.045	D	−0.30	D94	2.1
2.35	Y	11.95	0.05	A	−0.42	P98	2.3
1.9 (0.2).....	Y	12.15	0.04	D	−0.29	T99a	2.0
2.2 (0.2).....	Y	12.15	0.04	D	−0.29	T99b	2.0

REFERENCES.—AT90 = Anthony-Twarog et al. 1990, C92 = Castellani et al. 1992, C99 = Castellani et al. 1999, CC94 = Carraro & Chiosi 1994, D94 = Demarque et al. 1994, D99 = Dominguez et al. 1999, P98 = Pols et al. 1998, T99a = Twarog et al. 1999 employing Bertelli et al. 1994 isochrones, and T99b = Twarog et al. 1999 employing Schaller et al. 1992 and Schaerer et al. 1993 isochrones.

reddening may be an independent indication of a problem with the isochrone fitting. Column (6) lists the metallicity used in creating the isochrones. Since the metallicity of NGC 2420 is almost surely within or very close to the range -0.30 to -0.40 (Friel & Janes 1993), this column helps to identify where inappropriate stellar evolutionary models may have been applied. Column (7) lists the references. Column (8) lists the WD age that would be derived for the distance moduli and reddening listed in columns (3) and (4). These WD ages are not preferred in any way, but rather are meant to serve as a comparison with the stellar evolution models since nearly every study used a different distance modulus and reddening.

We now consider each of the isochrone fits listed in Table 3. While theoretical stellar evolution models differ in numerous ways, including the convective mixing length used in the near-surface regions, whether or not diffusion is included, the detailed translation from the theoretical temperature-luminosity plane to the observational color-magnitude plane, and in the prescription for convective core overshoot if used, there remains a clear difference between those studies that do and do not incorporate core convective overshoot.

For historical comparison, and since so many recent papers adopt some of the parameters derived by Anthony-Twarog et al. (1990), we report their results here, even though their cluster parameters (but not their photometry) are now superseded by other studies. As remarked above, Anthony-Twarog et al. found a problematic fit with VandenBerg's (1985) isochrones, from which they derived an age of 3.4 ± 0.6 Gyr and $(m - M)_V = 11.95$. They assumed [Fe/H] $= -0.4$ and $E(B-V) = 0.05$, both of which are reasonable values according to nearly all subsequent efforts. Anthony-Twarog et al. argued that the poor fit between their photometry and VandenBerg's models likely indicated the need for models including core convective overshoot. Given the development in stellar evolution modeling and input physics in the last fifteen years, particularly updated opacity tables, the application of VandenBerg (1985) models in the Anthony-Twarog et al. study serves more as a starting point for the issue of convective core overshoot than as a definitive statement. This isochrone age is also high by all modern estimates, as our discussion will reveal.

Castellani, Chieffi, & Straniero (1992) use canonical stellar models and derive a cluster age of 1.7 Gyr, with $E(B-V) = 0.02$ and $(m - M)_V = 11.95$. Unfortunately, these results cannot be directly compared to those of other groups since their study was meant as a test of theory, and they only compared the NGC 2420 photometry to solar metallicity isochrones. Nonetheless, their derived age is consistent with the most recent ages derived by other groups using canonical models.

Dominguez et al. (1999) concluded that the complex shape of the main-sequence turn-off region in NGC 2420 is not due to convective core overshoot, as argued by many others, but rather to the confusing photometric locations of multiple stars.[8] With this interpretation they derived an age of 1.6 ± 0.2 Gyr and $(m - M)_V = 12.19$. Dominguez et al. also noted the consistency of their isochrone age with the age implied by the coolest WDs we reported in Paper I.

Castellani, degl'Innocenti, & Marconi (1999), in a study of mixing length theory (surface convection) and models incorporating diffusion but not incorporating core convective overshoot, derive an age for NGC 2420 of 1.5 ± 0.1 Gyr, along with $E(B-V) \approx 0.16$, and $(m - M)_V = 12.4$. In this case, the high reddening and distance modulus make their age result suspect.

Carraro & Chiosi (1994) applied their convective core overshoot models to NGC 2420 and derived an age of 2.1 Gyr, $E(B-V) = 0.08$, and $(m - M)_V = 11.80$. For the reasons discussed above, their distance modulus may be too low, and their reddening value is likely to be modestly too high.

Demarque et al. (1994) fit the photometry of Anthony-Twarog et al. with their updated models with and without convective core overshoot. They concluded that the photometry required models with core overshoot, with an overshoot parameter $P_{\rm mix} = 0.23H_p$ and age $= 2.4 \pm 0.2$ Gyr. Their distance and reddening determinations, as discussed above, appear to be of high quality.

In a series of papers Pols and collaborators (Schroder, Pols, & Eggleton 1997; Pols et al. 1997; Pols et al. 1998) tested their canonical and overshoot models against giants of known mass, double-lined spectroscopic binaries, and open clusters. They recommend the use of convective core overshoot models for solar metallicity stars with main-sequence masses ≥ 1.5 solar masses. This limit of ≈ 1.5 solar masses scales inversely with metallicity and they note that for the metallicity of NGC 2420 the limit is probably slightly less than 1.4 solar masses. In their fit to NGC 2420 Pols et al. decisively favor the overshoot models and find an age of 2.35 Gyr and a turn-off mass of 1.47 solar masses, after adopting [Fe/H] $= -0.42$, $E(B-V) = 0.05$, and $(m - M)_V = 11.95$.

Twarog et al. (1999) find an age of 1.9 ± 0.2 or 2.2 ± 0.2 Gyr based on either the models of Bertelli et al. (1994) or Schaerer et al. (1993) and Schaller et al. (1992) respectively, all of which employ convective core overshoot. While the real goal of the Twarog et al. study was not to determine the isochrone age of NGC 2420, but rather to study the absolute magnitude of the red giant branch clump, their careful study appears to yield good isochrone fits, and good values for the cluster distance and reddening. While the Bertelli et al. isochrone age is the youngest overshoot age derived for NGC 2420, it is still older than any of the modern canonical isochrone fits.

In Figure 8 we present a summary of the modern stellar evolution isochrone ages for NGC 2420 along with our WD cooling age as a function of the assumed distance modulus. The solid line is our best-fit WD cooling age. The two dashed lines represent the ± 1 σ differences from our best age of 0.2 Gyr. The canonical isochrone ages are indicated by the open squares, whereas the convective overshoot isochrone ages are indicated by the filled circles. We use the age errors provided by the authors when given (see Table 3), and otherwise assume an age uncertainty of ± 0.2 Gyr. Most of the overshoot model ages agree with our WD cooling ages. The canonical models, on the other hand, produce ages that are generally in conflict with the WD cooling ages. The oldest canonical model clearly is inconsistent with the WD cooling ages, but this is the now-outdated model of VandenBerg (1985), and therefore the poor agree-

[8] The effect of multiple stars on the turn-off region can be independently verified by radial velocity techniques (e.g., Daniel et al. 1994), but this test has not yet been performed for NGC 2420.

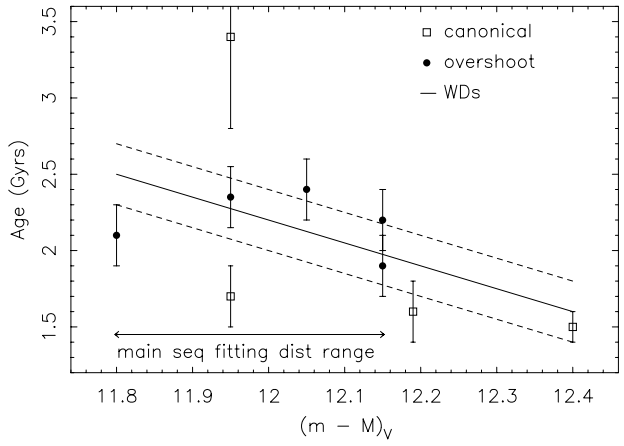

FIG. 8.—Comparison between all modern isochrone ages determined for NGC 2420 and our WD cooling age as a function of assumed distance modulus. The solid line is our best-fit WD cooling age. The two dashed lines represent the $\pm 1\ \sigma$ uncertainties of 0.2 Gyr. The canonical isochrone ages are plotted as open squares and the convective overshoot isochrone ages are plotted as filled circles.

ment is not surprising. The canonical model at $(m - M)_V = 11.95$ and 1.7 Gyr is from the Castellani et al. (1992) study employing solar metallicity isochrones, so the disagreement here is not surprising either. Of the remaining two canonical studies (Castellani et al. 1999 and Dominguez et al. 1999), both produce isochrone ages consistent with the WD cooling ages, though both employ high distance moduli. The distance discrepancy for the Dominguez et al. study may be minor, however.

As a final note on the comparison between isochrone and WD cooling ages, an incorrect distance modulus can inappropriately alter the assumed physics involved in stellar evolution, since the assumed stellar luminosity and thereby the assumed stellar mass depends on the assumed cluster distance. Therefore, the last word on the question of canonical versus core overshoot models for this cluster may have to await a precise and agreed-upon determination of the cluster distance modulus. In turn, a precise distance modulus is likely to require an improved cluster metallicity value. In the meantime, since both WD cooling ages and isochrone ages scale similarly with the assumed distance, we have applied the fairest comparison we can. Once a precise cluster distance modulus is determined, our WD photometry provides a strict consistency check of any isochrone fitting.

3.5. *The Limit of the Main Sequence*

While our observations were designed to measure the luminosities of the faintest cluster WDs, they also revealed a CMD that probes the cluster main sequence from $V = 16$ to 26. This apparent magnitude range corresponds to the mass range of 1.2 to 0.15 solar masses, based on the empirical mass-luminosity calibration of Henry & McCarthy (1993). We do not derive a cluster luminosity function or initial mass function from these data, as done by von Hippel et al. (1996) from the cycle 4 data, as the increase in numbers of stars does not warrant a reexamination of this subject. However, the deeper exposures and the larger field of view allowed us to detect candidate cluster main-sequence stars significantly fainter than those studied by von Hippel et al. (1996). Because of the current interest in comparing the photometric properties of faint main-sequence stars in clusters at different metallicity, we tabulate the main-sequence ridge line in Table 4. The ridge line was determined by fitting a fourth-order polynomial to the photometry for those stars that appear to lie along the well-represented portion of the single-star main sequence, between $M_V \approx 9$ to 14 ($V \approx 21$ to 26, mass ≈ 0.58 to 0.15 solar masses), assuming $(m - M)_V = 12.10$ and $E(B-V) = 0.04$. The quality of the fit can be seen by examining Figure 7*a*, where the ridge line is represented by plus symbols. We remind the reader that all of these stars are redder than the red limit of the Holtzman et al. (1995) photometric transformations, $V-I < 1.5$.

TABLE 4

MAIN-SEQUENCE RIDGE LINE

$V-I$ (1)	M_V (2)
1.8.....	8.66
1.9.....	9.06
2.0.....	9.49
2.1.....	9.95
2.2.....	10.42
2.3.....	10.89
2.4.....	11.36
2.5.....	11.82
2.6.....	12.25
2.7.....	12.66
2.8.....	13.02
2.9.....	13.33
3.0.....	13.59

We can make tentative comments about cluster members of even lower mass than 0.15 solar masses. At the faint limit of our photometry we found three objects that passed our I-band SExtractor stellarity index cut at 0.78 (with values of 0.87, 0.95, and 0.96), but which were too faint in the V band to provide a reliable centroid, and thus were rejected as poor matches between the V- and I-band photometry lists. These objects were measured to have $I \approx 23.8$, 24.6, and 24.7. These magnitudes are approximate due to their low signal-to-noise and uncertain color correction. The V-band photometry is even more uncertain. Table 5 lists the I- and V-band magnitudes for these three objects, along with their right ascension and declination (J2000.0). The brightest of these three objects is likely to be a cluster member, based on its position in the CMD. It is, in fact, the same color as and only 0.2 mag fainter than the two reddest main-sequence candidates plotted in our CMDs. The mass of this object, assuming it is a cluster member, is ≈ 0.12 solar masses, based on the calibration of Henry & McCarthy (1993). The two fainter objects, if cluster main-sequence stars, would have slightly lower mass, ≈ 0.11 solar masses. Since the

TABLE 5

FAINT RED STARS

ID (1)	I (2)	V (3)	R.A. (4)	Decl. (5)
MS1.....	23.8	26.9	7 38 30.94	21 34 44.9
MS2.....	24.6	27.5	7 38 31.62	21 36 37.3
MS3.....	24.7	...	7 38 23.74	21 35 30.4

completeness level at these faint magnitudes is only a few percent, it appears likely that NGC 2420 contains many very faint stars near the hydrogen-burning limit.

4. CONCLUSION

We have used deep *HST* WFPC2 observations of two fields in NGC 2420 to produce a cluster CMD down to $V \approx 27$. After imposing morphological selection criteria we find eight candidate white dwarfs in NGC 2420. Our completeness estimates indicate that we have found the terminus of the WD cooling sequence. We argue that the cluster distance modulus is likely to be close to 12.10 with $E(B-V) = 0.04$. With these parameters we find a white dwarf cooling age for NGC 2420 of 2.0 ± 0.20 ($1\ \sigma$) Gyr. The 0.20 Gyr uncertainty includes errors in the photometry, sequence fitting, precursor timescales, and theoretical WD cooling timescales.

We derive cluster WD ages for a variety of distances to directly compare the WD age with the many main-sequence evolution ages for NGC 2420. We find that most of the stellar evolution models that incorporate convective overshoot derive ages which agree with our WD cooling ages. The canonical models, on the other hand, largely produce ages that are in conflict with the WD cooling ages. An exception to this tendency is the canonical isochrone fit of Dominguez et al. (1999), which results in an age that is consistent with the WD cooling age, but with a distance modulus that may be too high. The final word on the question of canonical versus core overshoot models for this cluster may have to await a precise and agreed-upon determination of the cluster distance modulus, which in turn, will likely require an improved cluster metallicity value.

It is a pleasure to thank Ken Mighell for the use of the CCDCAP photometry package and for many useful consultations, and Andy Fruchter for guidance with the drizzle package. We thank Leandro Althaus, Brad Hansen, Jarrod Hurley, and Matt Wood for providing their computer-readable model calculations or code and for helpful guidance. We also thank Pierre Demarque for helpful guidance. Support for this work was provided by NASA through grant number GO-6424 from the Space Telescope Science Institute, which is operated by the Association of Universities for Research in Astronomy, Inc., under NASA contract NAS 5-26555. This research has made extensive use of NASA's Astrophysics Data System Abstract Service.

REFERENCES

Ahrens, T. J. 1999, Master's thesis, Florida Inst. Tech.
Anderson, J., & King, I. R. 1999, PASP, 111, 1095
Anthony-Twarog, B. J., Kaluzny, J., Shara, M. M., & Twarog, B. A. 1990, AJ, 99, 1504
Benvenuto, O. G., & Althaus, L. G. 1999, MNRAS, 303, 30
Bertelli, G., Bressan, A., Chiosi, C., Fagotto, F., & Nasi, E. 1994, A&AS, 106, 275
Bertin, E., & Arnouts, S. 1996, A&AS, 117, 393
Canuto, V. M. 1999, ApJ, 524, 311
Canuto, V. M., & Dubovikov, M. 1998, ApJ, 493, 834
Cardelli, J. A., Clayton, G. C., & Mathis, J. S. 1989, ApJ, 345, 245
Carraro, G., & Chiosi, C. 1994, A&A, 287, 761
Casertano, S., & Mutchler, M. 1998, WFPC2 Instrument Science Report, 98-02
Castellani, V., Chieffi, A., & Straniero, O. 1992, ApJS, 78, 517
Castellani, V., degl'Innocenti, S., & Marconi, M. 1999, MNRAS, 303, 265
Claver, C. F. 1995, Ph.D. thesis, Univ. Texas, Austin
Daniel, S. A., Latham, D. W., Mathieu, R. D., & Twarog, B. A. 1994, PASP, 106, 281
Demarque, P., Sarajedini, A., & Guo, X.-J. 1994, ApJ, 426, 165
Dominguez, I., Chieffi, A., Limongi, M., & Straniero, O. 1999, ApJ, 524, 226
Friel, E. D., & Janes, K. A. 1993, A&A, 267, 75
Fruchter, A. S., & Hook, R. N. 1998 (astro-ph/9808087)
Hansen, B. M. S. 1999, ApJ, 520, 680
Henry, T. J., & McCarthy, D. W. 1993, AJ, 106, 773
Holtzman, J. A., Burrows, C. J., Casertano, S., Hester, J. J., Watson, A. M., & Worthy, G. S. 1995, PASP, 107, 1065
Hurley, J. R., Pols, O. R., & Tout, C. A. 2000, MNRAS, 315, 543
Iben, I., & Tutukov, A. V. 1984, ApJ, 282, 615
Koester, D., & Reimers, D. 1985, A&A, 153, 260
———. 1996, A&A, 313, 810
Krist, J. 1995, in ASP Conf. Ser. 77, Astronomical Data Analysis Software and Systems IV, ed. R. A. Shaw, H. E. Payne, & J. J. E. Hayes (San Francisco: ASP), 349
Leggett, S. K., Ruiz, M. T., & Bergeron, P. 1998, ApJ, 497, 294
Liebert, J., Dahn, C. C., & Monet, D. G. 1988, ApJ, 332, 891
Mighell, K. J. 1997, AJ, 114, 1458
Oswalt, T. D., Smith, J. A., Wood, M. A., & Hintzen, P. 1996, Nature, 382, 692
Pinsonneault, M. H., Stauffer, J., Soderblom, D. R., King, J. R., & Hanson, R. B. 1998, ApJ, 504, 170
Pols, O. R., Schroder, K.-P., Hurley, J. R., Tout, C. A., & Eggleton, P. P. 1998, MNRAS, 298, 525
Pols, O. R., Tout, C. A., Schroder, K.-P., Eggleton, P. P., & Manners, J. 1997, MNRAS, 289, 869
Reid, I. N., & Majewski, S. R. 1993, ApJ, 409, 635
Reid, I. N., Yan, L., Majewski, S., Thompson, I., & Smail, I. 1996, AJ, 112, 1472
Richer, H. B., et al. 1997, ApJ, 484, 741
Richer, H. B., Fahlman, G. G., Rosvick, J., & Ibata, R. 1998, ApJ, 504, L91
Salaris, M., Dominguez, I., Garcia-Berro, E., Hernanz, M., Isern, J., & Mochkovitch, R. 1997, ApJ, 486, 413
Schaerer, D., Meynet, G., Maeder, A., & Schaller, G. 1993, A&AS, 98, 523
Schaller, G., Schaerer, D., Meynet, G., & Maeder, A. 1992, A&AS, 96, 269
Schroder, K.-P., Pols, O. R., & Eggleton, P. P. 1997, MNRAS, 285, 696
Schmidt, M. 1959, ApJ, 129, 243
Stetson, P. B. 1998, PASP, 110, 1448
Trimble, V., & Leonard, P. J. T. 1996, PASP, 108, 8
Twarog, B. A., Anthony-Twarog, B. J., & Bricker, A. R. 1999, AJ, 117, 1816
van Altena, W. F., & Jones, B. F. 1970, A&A, 8, 112
VandenBerg, D. A. 1985, ApJS, 58, 711
von Hippel, T. 1998, AJ, 115, 1536
von Hippel, T., Gilmore, G., & Jones, D. H. P. 1995, MNRAS, 273, L39 (Paper I)
von Hippel, T., Gilmore, G., Tanvir, N., Robinson, D., & Jones, D. H. P. 1996, AJ, 112, 192
von Hippel, T., & Sarajedini, A. 1998, AJ, 116, 1789
Whitmore, B., Heyer, I., & Casertano, S. 1999, PASP, 111, 1559
Winget, D. E., Hansen, C. J., Liebert, J., van Horn, H. M., Fontaine, G., Nather, R. E., Kepler, S. O., & Lamb, D. Q. 1987, ApJ, 315, L77
Wood, M. A. 1992, ApJ, 386, 539